Published in final edited form as:
Anal Chem. 2013 December 3; 85(23): 11545–11552. doi:10.1021/ac4030939.

Tunable-Delay Shunts for Paper Microfluidic Devices

Bhushan J. Toley, **Brittney McKenzie**, **Tinny Liang**, **Joshua R. Buser**, **Paul Yager**, and **Elain Fu**
Department of Bioengineering, University of Washington, Seattle, WA 98195

Abstract

We demonstrate a novel method for controlling fluid flow in paper-based devices. The method delays fluid progress through a porous channel by diverting fluid into an absorbent pad-based shunt placed into contact with the channel. Parameters to control the delay include the length and the thickness of the shunt. Using this method, reproducible delays ranging from 3 to 20 minutes were achieved. A simple electrical circuit model was presented and used to predict the delays in a system. Results from the model showed good agreement with experimental observations. Finally, the shunts were used for the sequential delivery of fluids to a detection zone in a point-of-care compatible folding card device using biochemical reagents for the amplified detection of the malaria protein *Pf*HRP2.

Keywords

Paper microfluidics; valve; 2DPN; point-of-care diagnostics; flow control; fluid flow modeling; electrical circuit

Introduction

The current standard diagnostic test format for low-resource settings is the lateral flow test (LFT). Though LFTs fulfill many of the ASSURED criteria[1], i.e. affordable, user-friendly, rapid, and equipment-free, they have been criticized for both their inability to assay for multiple analytes from a single biosample and their poor sensitivity for some analytes of clinical importance[2]. Addressing either of these issues in a simple paper[†]-based test format could have great utility, especially for applications in low-resource settings.

In 2008, the Whitesides group introduced microfluidic paper-based analytical devices (μPADS), two and three-dimensional paper-based structures that enable multiplexed colorimetric assays (e.g. for detection of glucose and protein)[3]. Subsequent work in the area of paper-based assay development has included demonstrating alternate fabrication methods[4], implementing multiplexed assays for the detection of additional biomarkers using

Correspondence to: Elain Fu, School of Chemical, Biological, and Environmental Engineering, Oregon State University, elain.fu@oregonstate.edu.

Supporting Information
Seven pieces of supporting information are available. First, a table of material properties is provided. Second, an experimental protocol for the demonstration of shunt compatibility with biochemical reagents in the context of *Pf*HRP2 detection is included. Third, details of an electrical circuit model of an absorbent pad-based shunt on a porous channel are presented. Fourth, an analytical solution for fluid progress through a porous material using Ohm's Law is presented. Fifth, both experimental and model results on the effect of spacer thickness on delay time in the folding card format are provided. Sixth, an experimental description of tracking fluid fronts in a system of cellulose and nitrocellulose is included. And seventh, additional model predictions on the effect of shunt material are provided. This supporting material is available free of charge via the Internet at http://pubs.acs.org.

[†]Here the term "paper" is used to broadly refer to porous materials including nitrocellulose used in conventional lateral flow tests.

one-step colorimetric reactions (e.g. nitrite, uric acid, and lactate)[5], or performing the simultaneous analysis of multiple controls for on-device calibration[6]. More recently, two-dimensional paper networks (2DPNs) for automated multi-step sample processing have been introduced. A key feature of the 2DPN assay is the configuration of the network, composed of multiple inlets per detection region, which functions as a program for the timed delivery of multiple reagent volumes within the network. 2DPNs have the ability to expand testing capability over LFTs to achieve improved test performance, e.g. a higher sensitivity. For example, 2DPNs that perform the processes of signal amplification[7,8], sample dilution and mixing[9], and small molecule extraction[9], have been demonstrated.

Critical to the operation of multi-step paper-based assays is a set of paper fluidic tools (i.e. analogs to the pump controls and valves[††] of conventional microfluidics) to manipulate fluids within the network for the precise timing of reagent delivery and metering of reagent volumes. A number of paper fluidic tools have been demonstrated. Channel geometry has been used to vary the flow velocity of fluids within the channel[10]. In a related effort, the geometry of the downstream wick, e.g. a fan shape, was used to produce quasi-steady flow in the channel upstream[11]. Several tools for switching-off fluid flow have been demonstrated. These include source pads of varying fluid capacity that release a well-defined volume of fluid into the channel[7,12] or inlets that are submerged by varying distances into a common well that disconnent from the well after a well-defined volume of fluid has passed[13]. Complementary to this, several tools for switching on fluid flow to a downstream location at a specific time have been demonstrated. One method uses a dissolvable sugar barrier to create delays of up to an hour. Another method relies on modification of the wetting properties of the channel through application of wax[14], or use of surfactant to bridge a hydrophobic region to create a diode valve[15]. Additional tools for switching on flow rely on simple user-activated mechanical means[16,17,18]. Most recently, several active methods for the switching on of flows have been developed, including eletrowetting of a dielectric in a porous channel[19] and the use of magnetically-actuated valves[20].

Our goal was to create a tool to complement existing methods. Like the other methods of switching on flows, it should be compatible with use in paper microfluidic devices and be easy to fabricate. In addition, a tool that requires no user intervention, does not involve the release of chemicals, and does not require any equipment to operate, would have value for certain applications. In the current report, we demonstrate a novel system of tunable delays for use in paper microfluidic devices that meets these criteria. We demonstrate the operation of this valving method, “shunts” in which fluid flow transiently follows two parallel paths, and the capability to produce a range of delays from 3 minutes to nearly 20 minutes. Control is achieved by varying parameters including the dimensions of the shunt material. Further, we present a simple electrical circuit model for the system and show how the model can be used to inform the design of a shunt with a desired delay. We characterize the shunts in a compact card format that is compatible with point-of-care use and demonstrate their operation through the sequential delivery of fluids.

Materials and Methods

“Paper” strips for all experiments were made from nitrocellulose membranes (FF80HP, *GE Healthcare*; Waukesha, WI). Absorbent pad-based shunts were made from cellulose CFSP223000 (*Millipore*, Billerica, MA) or cellulose 320 (*Ahlstrom*, Helsinki, Finland). Fluid source pads were made from glass fiber 8964 (*Ahlstrom*). All designs were drawn using the CAD program DraftSight (*Dassault Systemes HQ*, France) and parts were cut

[††]Here the term “valve” is used to broadly refer to a tool whose function is to regulate or control fluid flow in a channel.

using a 42-watt CO_2 laser cutter (*Universal Laser Systems*, Scottsdale, AZ). Some material properties can be found in the Supporting Information Section I.

A bench-top system was built for characterizing the range and reproducibility of the absorbent pad-based shunts (shown schematically in Fig. 2A). Nitrocellulose strips and cellulose pad shunts were attached to two separate transparent poly(methyl methacrylate) (PMMA) slabs using double adhesive backed 4-mil Mylar sheets (*Fralock*, Valencia, CA). The strips and pads were so arranged that when the PMMA slabs were placed together, the cellulose pads made contact with the nitrocellulose strips at the desired locations. Screws were used to hold the assembly together. Each device contained one control strip without a pad and four strips with pads. The nitrocellulose strips were 108 mm long and 4.6 mm wide and the cellulose pads were 7.6 mm, 15.2 mm, 22.9 mm, or 30.5 mm long, and 4.6 mm wide. A 19.1 mm thick black PMMA block with a fluid reservoir etched into the top surface served as a base for the assembly. Specifically, the assembly was placed onto the base such that the inlets of the nitrocellulose strips extending out from one edge of the assembly were submerged in the fluid reservoir. A 1- mg/ml solution of phenol red, adjusted to pH 7.0, was added to the reservoir and used to visualize the transport of the fluid front. Using a custom-designed humidity chamber, a device, surrounded by multiple sources of water, was equilibrated to a relative humidity of 75% before introduction of any fluids into the device.

The absorbent pad-based shunts were also incorporated into folding cards, a format appropriate for POC use (one version is shown schematically in Fig. 3A). The cards were fabricated from adhesive backed 10-mil Mylar (*Fralock*, Valencia, CA). Nitrocellulose strips and cellulose pads, a single layer of 15.2 mm long CFSP223000, were attached to adjacent sides of the card. The lengths and widths of the nitrocellulose and cellulose were otherwise equal to those in the bench-top system. On folding, the cards sealed closed as a result of the adhesion of regions between the strips and around the edges of the card. For characterization of the delays in the card format, a control strip and four nitrocellulose strips with identical pads were incorporated within a single card. The inlets of the nitrocellulose strips, extending out from one edge of the card, were dipped into a fluid reservoir prior to imaging. Humidity was controlled in these experiments as described above.

For the sequential delivery of fluids in the card format, nitrocellulose strips were completely contained within the folding card and glass fiber was used to create source pads. Cards with two folding flaps were fabricated – cellulose pads were attached to one flap and source pads were attached to the second flap. Different volumes of fluids to be sequentially delivered to a detection zone were pipetted onto the source pads before folding. The flap containing the cellulose pads was folded first to establish contact between the cellulose pads and the nitrocellulose. The second flap, containing the source pads, was folded to initiate the simultaneous flow of fluids into the nitrocellulose. A cellulose wicking pad was placed downstream of the detection zone to collect the fluids. Colored fluids--red and yellow food coloring (*The Kroger Co.*, Cincinnati, OH) and a solution of phenol red (*Sigma-Aldrich*, St. Louis, MO)--were used to visualize the timing and uniformity of sequential fluid delivery to the detection zone. Rough estimates of the fluid volumes delivered were made as follows. The lengths of the red regions in the montages were assumed to correspond to the total volumes of the red fluid delivered in each case - 12 ul for the device with shunts, and 8 ul for the device without shunts. Approximate volumes of the yellow and pink fluids that flowed over the detection zone were accordingly estimated by measuring the lengths of the yellow and pink regions in the respective montages. The same device design was then used to demonstrate the compatibility of the shunts with biochemical reagents. Details of the reagent list (*Pf*HRP2 antigen detection) have previously been published[8]; see Supporting Information Section II for the specifics of the protocol used in this study.

Images of flow through a device were acquired using a Logitech Pro 9000 (*Logitech*, Newark, CA) webcam operated using HandyAvi (*AZcendant*, Tempe, AZ) software. The position of the fluid front as a function of time was measured using ImageJ (NIH Research Services Branch). The fluid fronts had V-shaped profiles with two leading regions along the edges and a lagging region along the center. For consistency, in this study the location of the fluid front was taken to be at the lagging region. The error bars on the experimental data represent one standard deviation. Statistical comparisons were made using a two-tailed Student's t-test in Microsoft Excel (*Microsoft*, Redmond, WA). For the sequential delivery experiments, images were acquired every 2 seconds. A time series montage of a 2.3 mm×3.0 mm region (scaled 0.02× in one dimension) slightly upstream of the wicking pad was created using ImageJ.

Electrical circuit equations were solved in MATLAB (*Mathworks*, Natick, MA). The circuit model consisted of a system of algebraic-integral equations with time-dependent resistances and voltages (see Supporting Information Section III), and was solved to calculate electrical currents as a function of time. The equations were discretized in time and the integral terms were approximated using the trapezoidal rule to yield a system of algebraic equations. An intrinsic method was utilized to avoid numerical instability. The resulting system of nonlinear equations was solved at each time step using the Matlab *fsolve* function. For the estimation of error in the calculation of the delay by the model for a given combination of channel and shunt materials, the errors in the measurement of material properties – absorption capacity, permeability (inversely related to the fluidic resistance), and capillary pressure, were taken into account. Specifically, upper and lower limits of delay predictions by the model were obtained by inputting lower and upper limits of these parameters into the model; these errors were then plotted as error bars on the model results.

Results and Discussion

Shunts Using Absorbent Pads

Fluid introduced at one end of a strip of a porous material, such as nitrocellulose, flows into the strip as a result of capillary forces exerted at the liquid-air-solid interface along the fluid front (Fig. 1A). The rate of fluid flow through the material of the main channel, in this case nitrocellulose, may be altered by placing a shunt made out of an absorbent material--in this case cellulose--into contact with the main channel (Fig. 1B). Specifically, a portion of the fluid from the main channel is diverted into the shunt material, producing a delay in the progress of the fluid front to downstream locations of the main channel. In the absence of the shunt, the distance traveled by the fluid front will follow the Washburn equation[21,22] and is represented by a straight line on a distance vs. square root of time plot (**ab**; schematic of Fig. 1C). In the presence of the shunt, the fluid front follows this same trajectory before reaching the shunt (**ac**; Fig. 1C). After reaching the shunt, the absorption of fluid by the shunt material slows down the progress of the fluid front in the channel (**cd**; Fig. 1C). In time, the fluid front transits the shunt and its velocity increases again (**de**; Fig. 1C). The presence of the shunt causes a net delay, Δt, in the time required for the fluid front to reach the end of the main channel, represented by **be** (Fig. 1C).

The flow of fluid through a porous material is analogous to the flow of electrons in an electrical circuit[22,23]. For example, a length of dry porous material with a fluid source at one end may be represented by an electrical circuit, where the voltage V, is analogous to the capillary force generated by the porous material, the electrical resistance, $R(t)$, is analogous to the fluidic resistance of the material at time t after the fluid source is introduced, and the current, $i(t)$ is analogous to the flow rate of fluid through the porous material (Fig. 1D). An analytical solution of the electrical circuit equations produces the linear relationship between distance traveled and the square root of time that is observed experimentally as Washburn

flow, indicating that the model accurately predicts the progress of fluid through a porous material channel (see Supporting Information Section IV). The electrical circuit analogy can be extended to the shunt system composed of a porous material main channel in contact with a different porous material shunt (circuit of Fig. 1E). The assembly can be represented by two parallel branches of the circuit with different voltage sources and resistances for the shunt and the main channel. The values of the voltages in this circuit depend on the location of the fluid front. Specifically, a fully wetted section has no ability to imbibe fluid and is represented by a zero voltage, while any section that has a capacity for imbibition is represented by a non-zero voltage. Similarly, the resistance of each branch in the circuit is proportional to the amount of fluid that has passed through that branch, until the section becomes fully wet. A step-by-step progression of fluid through this system and its equivalent electrical circuit at each stage is provided in Supporting Information Section III.

Tuning Delays

The delays of the shunts can be tuned by changing the dimensions of the shunts, length or thickness, of a given material. First, delays produced using nitrocellulose (FF80HP) as the main channel and different lengths of cellulose (CFSP223000) shunts were measured using the bench-top system (Fig. 2A). A delay was defined as the difference in time required for the fluid front to reach the end of a nitrocellulose channel containing a cellulose shunt, compared to a control, the nitrocellulose channel only. The image series shows that increasing the length of the shunt increased the delay (Fig. 2B). A plot of the progress of the fluid fronts though the material indicates the behavior described above (Fig. 2C). Specifically, after reaching the cellulose shunt, progress of the fluid front deviated from the initial Washburn behavior in the nitrocellulose with significantly slowed progress, i.e. decreased slope relative to the initial slope of the distance vs. square root of time plot. Then, once the fluid front was in the nitrocellulose downstream of the shunt, the slope increased to near the initial slope. The resulting delay increased as the length of the shunt was increased (Fig. 2D). Distinct delays, between 200 s and 750 s (*; $P<10^{-4}$; N=4), were demonstrated by changing the shunt length in 7.6 mm increments. For each shunt length, the delays were reproducible with coefficients of variation (CV) ranging from 3.8% to 8.0%.

The delay can also be varied by changing the thickness of a shunt while maintaining constant length. The bench-top system was used to measure the delays produced by implementing shunts formed from one, two, and three layers of 15.2 mm long cellulose (CFSP223000) (Fig. 2E,F). Distinct delays, ranging from 319 s to 1055 s (*; $P<10^{-6}$; N=4), were obtained by varying the number of cellulose layers between one and three. For these delays, the CVs were between 1.4% and 5.9%. Note that alternate materials may also be chosen to increase the delays further if desired. However, producing very long delays may not be desirable in the context of minimizing assay time to result.

Incorporation of Shunts in Folding Cards for POC Use

The shunts were demonstrated in a folding card format compatible with POC use (Fig. 3A), and the reproducibility of the delays was characterized. For three runs of a card with 10-mil thick spacers, the normalized delays produced by the 15.2 mm long shunts were consistent across all runs at each strip position (Fig. 3C). In order to vary the magnitude of the delay, the length or thickness of the shunt may be adjusted, as was demonstrated in the bench-top system. The delay can also be varied by changing the thickness of the spacer in the card (see Supporting Information Section V).

Model predictions and comparison with experimental results

The electrical circuit model was used to predict the locations of the fluid fronts in a system of a nitrocellulose (FF80HP) channel and a cellulose CFSP223000 shunt as a function of

time (Fig. 4A). The cellulose shunt in this model had a 2.5-fold greater absorption capacity, a 0.5-fold greater fluidic resistance, and a 1.1-fold greater capillary force than the nitrocellulose channel. These model input parameters were consistent with the experimentally measured values for the permeability, capillary pressure, wicking rate, and absorption capacity of the nitrocellulose and cellulose (Table S1 and the discussion following it). The model predictions (Fig. 4A) agreed well qualitatively with the experimental results for the system (Fig. 4B, see Supporting Information Section VI for a description of the experiment). First, the model predicted the experimentally observed decrease in velocity of the fluid fronts in cellulose and nitrocellulose within the shunt region. Second, the model predicted the faster progress of the fluid front through the cellulose as compared to the nitrocellulose. And third, the model predicted the increase in velocity of the fluid front in nitrocellulose after the cellulose shunt was saturated.

The model was used to predict the delay dependence for different lengths and number of layers in the cellulose CFSP223000 shunt. In each case, a single model parameter was varied from the nominal value described above (used for the solution of Fig. 4A). The predicted delays corresponding to the nominal case are highlighted as dark circles (Fig. 4C-D). The model predicted that as the length of the shunt is increased, the delay produced increases (Fig. 4C), in qualitative agreement with the experimental results of Fig. 2D. Similarly, the model showed that as the capacity, or thickness, of the shunt is increased, the delay produced increased (Fig. 4D). This trend was also experimentally observed in measurements of the delays produced by stacking multiple layers of absorbent material to create the shunts (Fig. 2F).

The electrical circuit model was also used to qualitatively predict the effect of material properties on the resulting delays. The capillary force and fluidic resistance of a porous material are interrelated in that changing the pore structure of a material changes both of these parameters for a given fluid. The combined effect of the variation of the capillary force and fluidic resistance on delays can be represented by a map as shown in Fig. 4E (see Supporting Information Section VII for model predictions on the delay for each of these independently). Each point on this map corresponds to a particular combination of capillary force and fluidic resistance that may be associated with a given set of materials and fluid. The map shows that for a shunt having a 2.5- fold higher absorption capacity than the channel material, the maximum delay would be achieved with a shunt material that generates an equal capillary force as the channel material, but with a 0.4-fold smaller fluidic resistance than the channel material (gray circle; Fig. 4E).

The electrical circuit model can be used as a design tool to obtain qualitative predictions on the delay for a different shunt material. For example, the model can be used to predict how the delay will change from the case of the cellulose CFSP223000 shunt with the nitrocellulose channel (fluid is water), when an alternate cellulose material with a higher absorption capacity such as cellulose 320, is used for the shunt. The model parameters were the same as for the nominal case (Fig. 4A), except the material properties of the shunt were adjusted to reflect the experimentally measured properties for cellulose 320 (Table S1). Specifically, model parameters for cellulose 320 were estimated by scaling the corresponding model parameters for cellulose CFSP223000 using the ratio of measured properties as scaling factors. The model predicted that the delay would increase (left white *vs.* gray bars; Fig. 4F) for cellulose 320 as compared to cellulose CFSP223000. This agreed qualitatively with experimental results (right white *vs.* gray bars; Fig 4F), (*; $P<0.05$; $N=4$; Fig. 4F). However, the model underestimated the increase in the delay compared to the experimentally observed increase in the delay. A reason for this may be that the physical thickness used as an input for the model overestimated the cross-sectional area used for wicking, and thus the model prediction for the increase in the delay is low. The model

prediction can be made to match the increase observed in the experimental results (left white vs. hashed bar; Fig. 4F) when an effective thickness of 1.6 mm (compared to the measured thickness of 2.7 mm; Table S1) is used to estimate the capillary force. The errors bars in the estimation of delay by the model represent the uncertainty in the measurement of the material properties input into the model.

Sequential Fluid Delivery in Folding Cards

Sequential delivery of fluids to a detection zone using cellulose (CFSP223000) shunts was demonstrated, first for a system of three colored fluids, and second in an immunoassay for the detection of the malaria protein *Pf*HRP2. The device had three legs, each connected to a different fluid source. The first leg did not contain a shunt. The second and third legs contained 5.1 mm and 20.3 mm long shunts (dotted green lines; Fig. 5A). A double folding card format was used in which the first fold established contact between the cellulose shunts and nitrocellulose channels, and the second fold established contact between the source pads and the channels. In the example here, 12 μl of red, 20 μl of yellow, and 80 μl of pink colored fluid were automatically delivered to the detection zone. The image series, at 0, 0.2, 4.2, and 10.7 minutes after completing the double fold, shows the introduction of fluids into the device inlets, and the arrival of red fluid, yellow fluid, and pink fluids to the detection zone (Fig. 5A). A montage of time-lapse images of the detection zone shows the timing and the relative volumes of the three fluids delivered up to a time of 19.3 minutes (Fig. 5B). Note that in this design, the sequential delivery of fluids to the detection zone was enabled both by the shunts and the geometry of the inlet legs, i.e. different lengths of the input legs. Though sequential delivery can be achieved using geometry only[24], a significant advantage of using the absorbent pad-based shunts is the capability to deliver larger volumes of fluid using the same device footprint. Specifically, in a device with the same footprint but without shunts, only smaller volumes of the red (8 μl) and yellow (15 μl) fluids could be delivered sequentially (and a larger volume of pink fluid in the same time of 19.3 minutes, Fig. 5C vs. Fig 5B). An attempt to load larger volumes led to premature delivery of fluids from legs 2 and 3 to the detection zone.

The compatibility of the shunts with biochemical reagents from a signal amplified assay for *Pf*HRP2 was then demonstrated. The same device design was used to sequentially deliver 12 μl of sample plus a gold nanoparticle-antibody conjugate, 20 μl of a rinse solution, and 80 μl of a gold enhancement solution to a detection zone (Fig. 5D). A light pink signal could be seen in the detection zone 15 minutes after the passage of the conjugate (leg 1) and rinse (leg 2) solutions (Fig. 5D); this is analogous to the signal obtained from the steps in a conventional lateral flow test. This signal was then amplified by the delivery of the gold enhancement solution from the third leg of the device, producing a dark blue-black signal at 40 minutes (Fig. 5D).

These absorbent pad-based shunts have several potential advantages over previously developed valving methods. These shunts can reduce the device footprint compared to devices that use geometry only (e.g. varying the path lengths from the sources to the detection zone to deliver fluids sequentially). In contrast to dissolvable barriers or hydrophobic barriers, there are no chemicals applied to the porous substrate that might then have a negative impact on downstream device processes. Though these shunts introduce additional volume into the fluid path, in the folding card device of Figure 5, in which small fluid volumes in source pads feed into the network and the cellulose wicking pad is significantly larger in fluid capacity than the cellulose shunts, the fluid volume retained in the network is expected to be small. Moreover, when storing reagents dry on the device for rehydration at the time of use, the dry reagents may be incorporated downstream of any cellulose shunts, so that waste of potentially expensive reagents is not an issue. Future work

includes demonstration of the utility of the shunts in an assay, as well as quantification of the effects of varying environmental conditions, i.e. humidity levels and temperature on device operation.

Conclusion

We have demonstrated a novel tunable shunt for use in paper microfluidic devices. Such shunts are capable of producing delays, ranging from 3 minutes to close to 20 minutes, using control parameters such as the dimensions of the absorbent material of the shunt. We have also presented a simple electrical circuit model that can be used as a design tool for creating absorbent pad-based shunts with the desired properties for a given application. These shunts are compatible with a compact card format suitable for point-of-care use and were demonstrated to perform sequential delivery in the context of an amplified immunoassay.

Supplementary Material

Refer to Web version on PubMed Central for supplementary material.

Acknowledgments

We would like to thank Barry Lutz, Ryan Gallagher, Josh Bishop, Luke Allpress, and Nuttada Panpradist for stimulating discussions and technical assistance throughout the course of this work. The research reported in this publication was supported by the Defense Advanced Research Projects Agency under Grant Number HR0011-11-2-0007 and the National Institute of Allergy and Infectious Disease of the National Institutes of Health under Award Number R01AI096184. B.M. acknowledges the Washington NASA Space Grant Consortium, the University of Washington Department of Bioengineering, the Mary Gates Endowment, the Pacific Northwest LSAMP, and the University of Washington GenOM Project (National Institutes of Health under Award Number HG02360-12, Genentech Foundation, Washington Research Foundation) for their support. T.L. acknowledges support from the National Science Foundation Graduate Research Fellowship under Grant Number DGE-1256082. The content is solely the responsibility of the authors and does not necessarily represent the official views of the National Institutes of Health.

References

1. Kettler, H.; White, K.; Hawkes, S. The World Health Organization. 2004.
2. Posthuma-Trumpie GA, Korf J, van Amerongen A. Analytical and Bioanalytical Chemistry. 2009; 393:569–582. [PubMed: 18696055] O'Farrell, B. Lateral Flow Immunoassay. Wong, R.; Tse, H., editors. Humana Press; New York: 2009. p. 1-33.
3. Martinez AW, Phillips ST, Butte MJ, Whitesides GM. Angewandte Chemie- International Edition. 2007; 46:1318–1320.Martinez AW, Phillips ST, Whitesides GM. Proceedings of the National Academy of Sciences of the United States of America. 2008; 105:19606–19611. [PubMed: 19064929]
4. Abe K, Kotera K, Suzuki K, Citterio D. Analytical and Bioanalytical Chemistry. 2008; 398:885–889. [PubMed: 20652543] Fenton E, Mascarenas M, Lopez G, Sibbett S. Applied Materials and Interfaces. 2009; 1:124–129. [PubMed: 20355763]
5. Li X, Tian JF, Shen W. Analytical and Bioanalytical Chemistry. 2010; 396:495–501. [PubMed: 19838826] Dungchai W, Chailapakul O, Henry CS. Analytica Chimica Acta. 2010; 674:227–233. [PubMed: 20678634]
6. Wang W, Wu WY, Wang W, Zhu JJ. Journal of Chromatography A. 2010; 1217:3896–3899. [PubMed: 20444459]
7. Fu E, Kauffman P, Lutz B, Yager P. Sensors and Actuators B-Chemical. 2010; 149:325–328.
8. Fu E, Liang T, Houghtaling J, Ramachandran S, Ramsey SA, Lutz B, Yager P. Analytical Chemistry. 2011; 83:7941–7946. [PubMed: 21936486] Fu E, Liang T, Spicar-Mihalic P, Houghtaling J, Ramachandran S, Yager P. Analytical Chemistry. 2012; 84:4574–4579. [PubMed: 22537313]

9. Osborn J, Lutz B, Fu E, Kauffman P, Stevens D, Yager P. Lab on a Chip. 2010; 10:2659–2665. [PubMed: 20680208]
10. Fu E, Lutz B, Kauffman P, Yager P. Lab on a Chip. 2010; 10:918–992. [PubMed: 20300678] Fu E, Ramsey SA, Kauffman P, Lutz B, Yager P. Microfluidics and Nanofluidics. 2011; 10:29–23. [PubMed: 22140373] Kauffman P, Fu E, Lutz B, Yager P. Lab on a Chip. 2010; 10:2614–2617. [PubMed: 20676410]
11. Mendez S, Fenton EM, Gallegos GR, Petsev DN, Sibbett SS, Stone HA, Zhang Y, López GP. Langmuir. 2010; 26:1380–1385. [PubMed: 19845342]
12. Fu E, Liang T, Houghtaling J, Ramachandran S, Ramsey SA, Lutz B, Yager P. Analytical Chemistry. 2011; 83:7941–7946. [PubMed: 21936486]
13. Lutz BR, Trinh P, Ball C, Fu E, Yager P. Lab Chip. 2011; 11:4274–4278. [PubMed: 22037591]
14. Noh N, Phillips ST. Analytical Chemistry. 2010; 82:4181–4187. [PubMed: 20411969]
15. Chen H, Cogswell J, Anagnostopoulos C, Faghri M. Lab Chip. 2012; 12:2909–2913. [PubMed: 22699228]
16. Martinez AW, Phillips ST, Nie Z, Cheng CM, Carrilho E, Wiley BJ, Whitesides GM. Lab Chip. 2010; 10:2499–2504. [PubMed: 20672179]
17. Li X, Tian J, Nguyen T, Shen W. Anal Chem. 2008; 80:9131–9134. [PubMed: 19551982]
18. Liu H, Li X, Crooks RM. Anal Chem. 2013; 85:4263–4267. [PubMed: 23586896]
19. Koo CK, He F, Nugen SR. Analyst. 2013; 138:4998–5004. [PubMed: 23828822]
20. Li X, Zwanenburg P, Liu X. Lab on a chip. 2013; 13:2609–2614. [PubMed: 23584207]
21. Washburn EW. Physical Review. 1921; 17:273–283.
22. Fu EL, Ramsey S, Kauffman P, Lutz B, Yager P. Microfluidics and Nanofluidics. 2011; 10:29–35. [PubMed: 22140373]
23. Dharmaraja S, Lafleur L, Byrnes S, Kauffman P, Buser J, Toley B, Fu E, Yager P, Lutz B. Programming paper networks for point of care diagnostics. 2013
24. Fu E, Lutz B, Kauffman P, Yager P. Lab on a Chip. 2010; 10:918–992. [PubMed: 20300678] Fu E, Liang T, Spicar-Mihalic P, Houghtaling J, Ramachandran S, Yager P. Anal Chem. 2012; 84:4574–4579. [PubMed: 22537313]

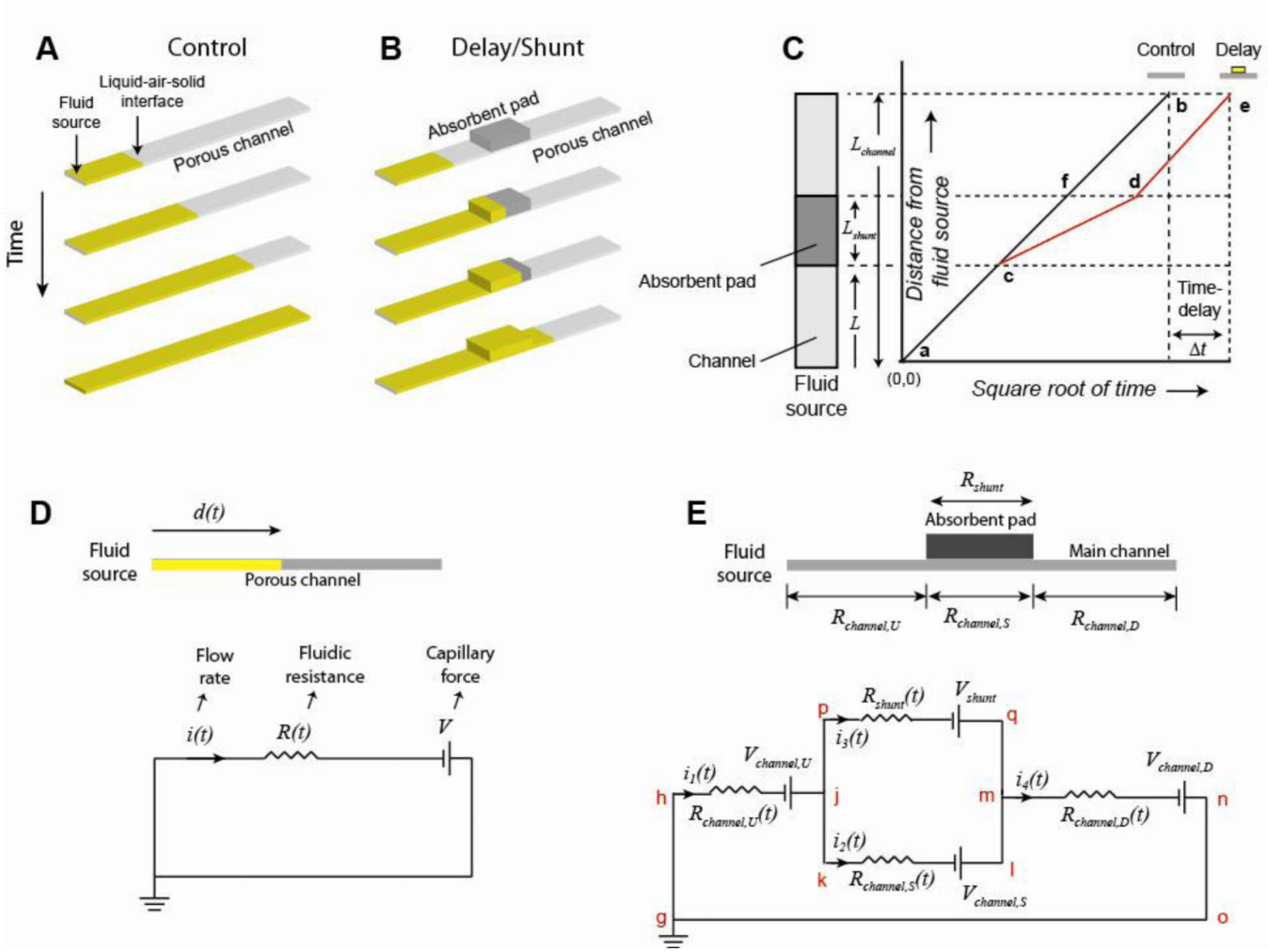

Figure 1.

Delays using absorbent pads as shunts: concept and electrical circuit analogy. **A-B**. The flow of fluid through a channel of a porous membrane in the absence (control; **A**) and in the presence (**B**) of a shunt. **C**. Schematic showing an idealized plot of the distance traveled by the fluid front as a function of square root of time. For the control with no shunt, fluid progression follows a straight line, as predicted by the Washburn equation. When a shunt is present, fluid progression deviates from Washburn flow, and there is a net delay, Δt, in the progress of the fluid front compared to the control. Depending on the net fluidic resistance offered by the assembly of the shunt placed over the main channel, compared to the channel of porous material alone, **de** may be either parallel to **fb** (approximately equal net resistance, when the resistance of the absorbent shunt material is much greater than the resistance of the main channel material) or may have a greater slope (lower net resistance) compared to **fb**. **D**. The electrical circuit analogy of fluid flow through a porous channel. **E**. The electrical circuit analogy of fluid flow through an assembly of an absorbent pad-based shunt in contact with a porous main channel. See Supporting Information Section III for a detailed description of this circuit.

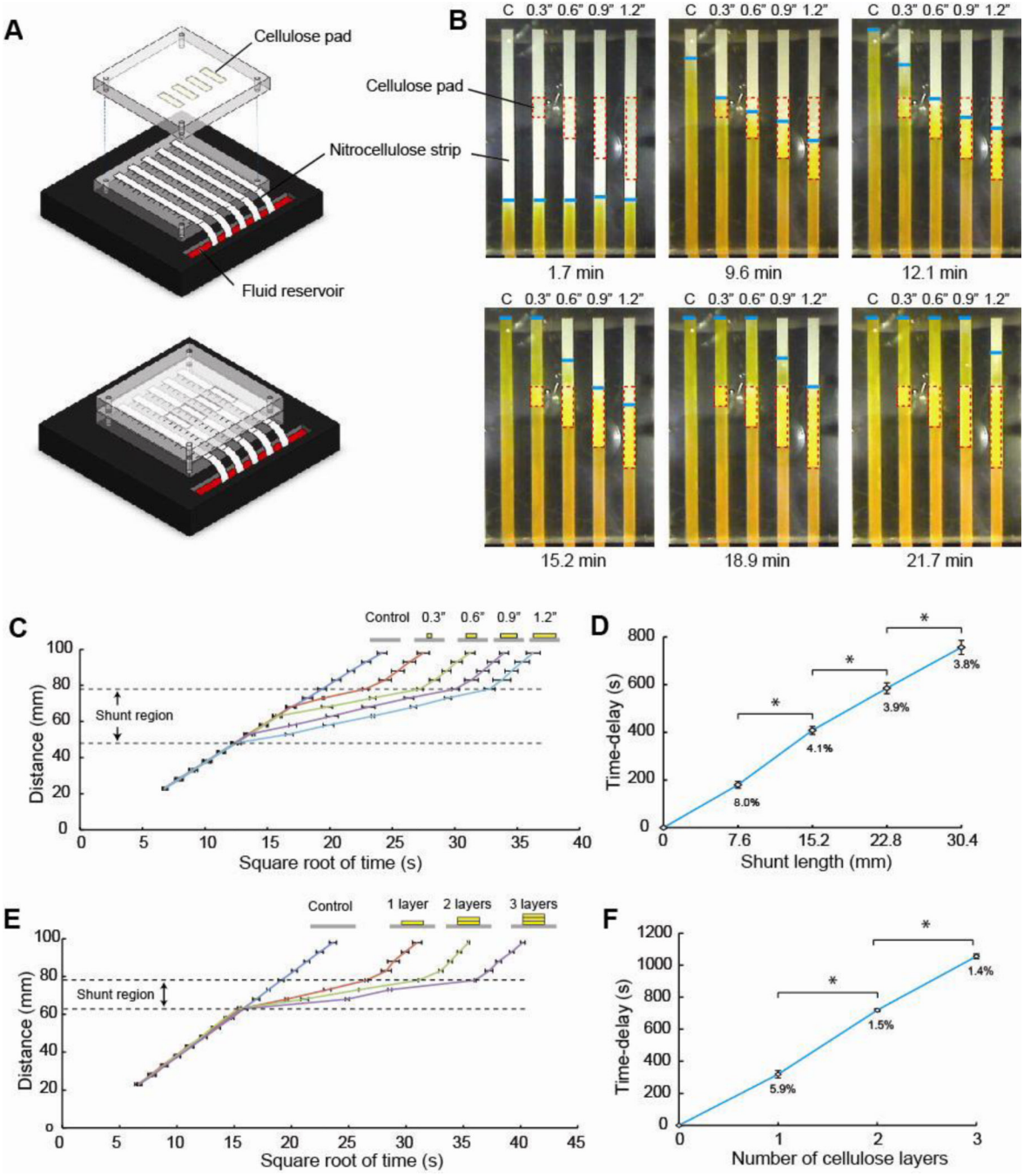

Figure 2.

Effect of shunt length and thickness on the magnitude of the delay. **A**. Schematic of the bench-top system used for measuring delays. **B**. Time-lapse images of the flow of fluid through nitrocellulose strips in the absence of (control) and in contact with 7.6 mm, 15.2 mm, 22.9 mm, and 30.5 mm shunts of cellulose CFSP223000. Dotted red lines indicate the location of the cellulose shunts and the blue lines mark the fluid fronts. Longer shunts produced longer delays. **C,E**. Plots of the distance traveled by the fluid front as a function of the square root of time for a nitrocellulose strip in contact with cellulose CFSP223000 shunts of different lengths (N=4) (**C**), and multiple layers of cellulose of length 15.2 mm

(N=4) (**E**). **D,F**. Plots of the delays produced by cellulose shunts as a function of shunt length (**D**), and number of layers in the shunt (**F**). Percent values represent the coefficient of variation.

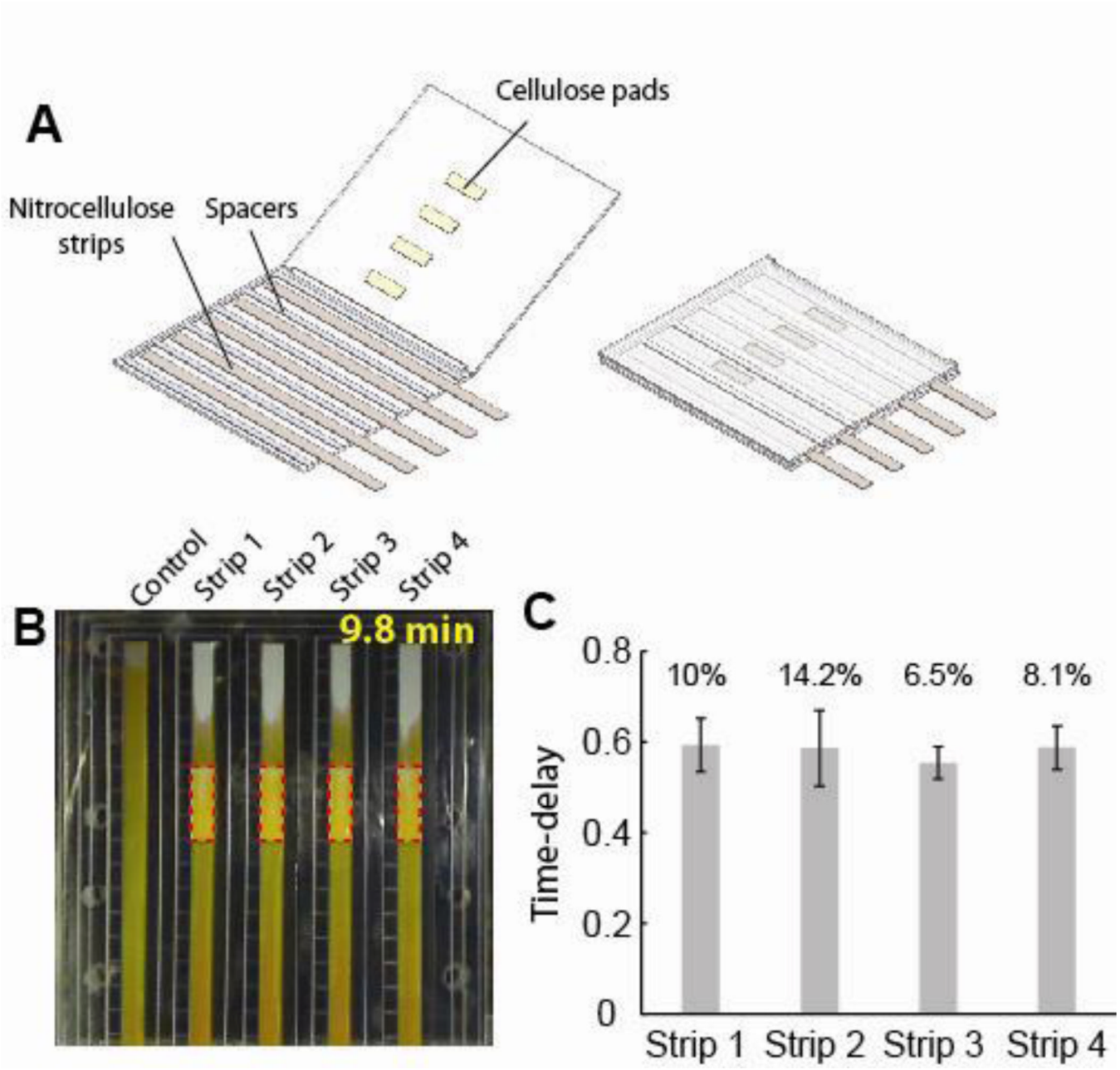

Figure 3.

Shunts in a POC-compatible folding card. **A**. Schematic of the folding card format. **B**. Image of the progress of fluid through nitrocellulose strips in the absence of (control) and in contact with 15.2 mm long cellulose CFSP223000 shunts. Fluid flow in the nitrocellulose channel was delayed by the presence of a cellulose shunt. **C**. Delays obtained at different strip locations within the cards. The mean delay is plotted at each location across multiple cards (N=3). The error bar is the standard deviation and percent values represent coefficients of variation.

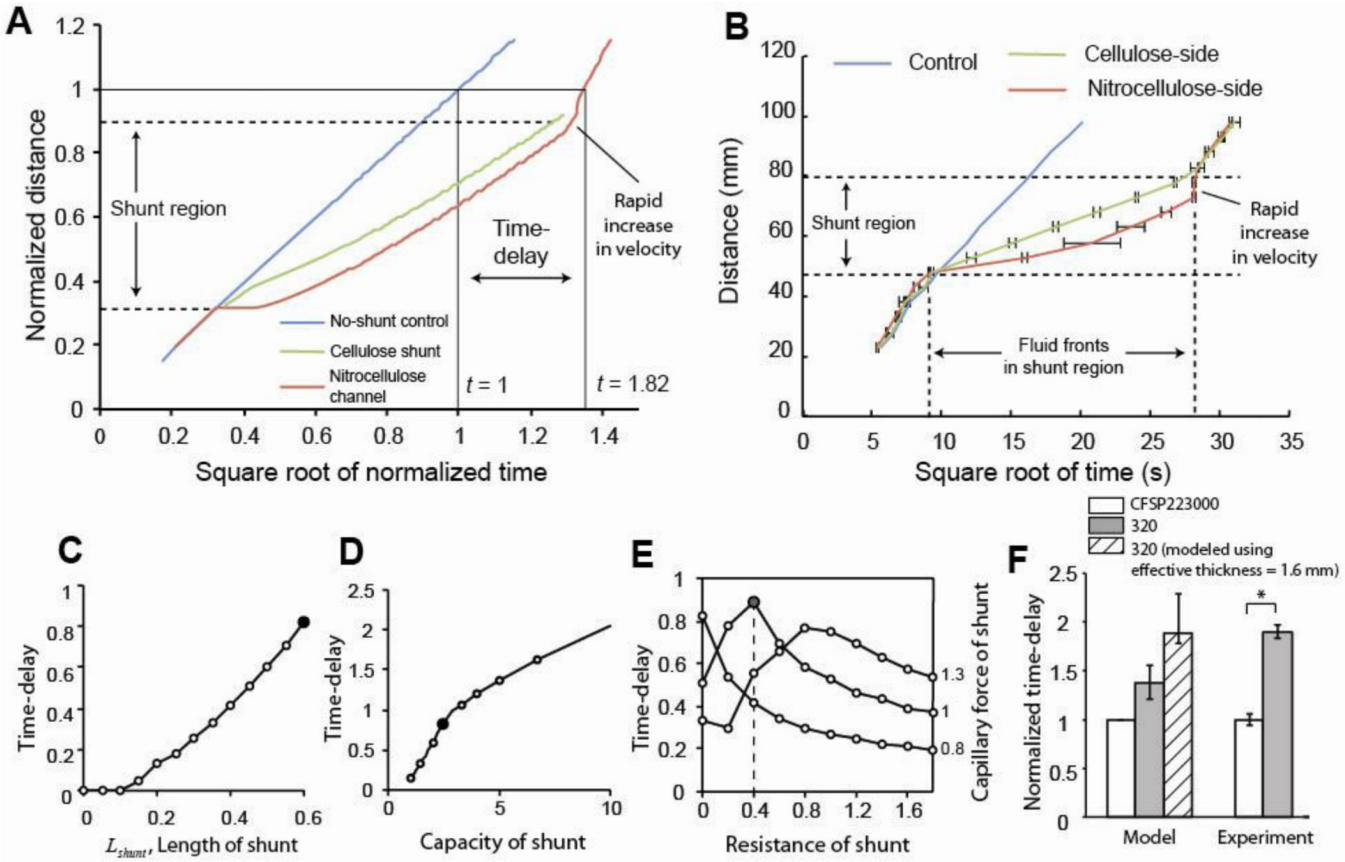

Figure 4.

Model predictions and comparison with experimental results. **A**. Locations of fluid fronts in a control of nitrocellulose channel only (blue line), a nitrocellulose channel in contact with a 33.0 mm cellulose shunt (red line), and a cellulose shunt (green line) that is in contact with a nitrocellulose channel, as a function of square root of time, as predicted by the electrical circuit model. **B**. Experimental results of the locations of fluid fronts plotted as a function of the square root of time for a control, and the two opposite-facing assemblies. In the shunt region, the fluid front in nitrocellulose lagged the fluid front in the cellulose. There was a rapid increase in the velocity of the fluid front in the nitrocellulose after the cellulose was fully wetted. There was good agreement between model predictions (**A**) and experimental observations (**B**). **C**. The model predicts that increasing the length of the cellulose increases the delay as experimentally observed (Fig. 2D). **D**. The model predicts that increasing the capacity of the cellulose increases the delay as experimentally observed (Fig. 2F). The solid data points represent the nominal case. **E**. Resistance-voltage map for predicting delays. Each point on this map corresponds to a combination of these two properties and predicts the values of the properties for maximizing the delays (solid data point). **F**. Comparison of model and experimental results for the delays generated by 15.2 mm long cellulose CFSP223000 and cellulose 320.

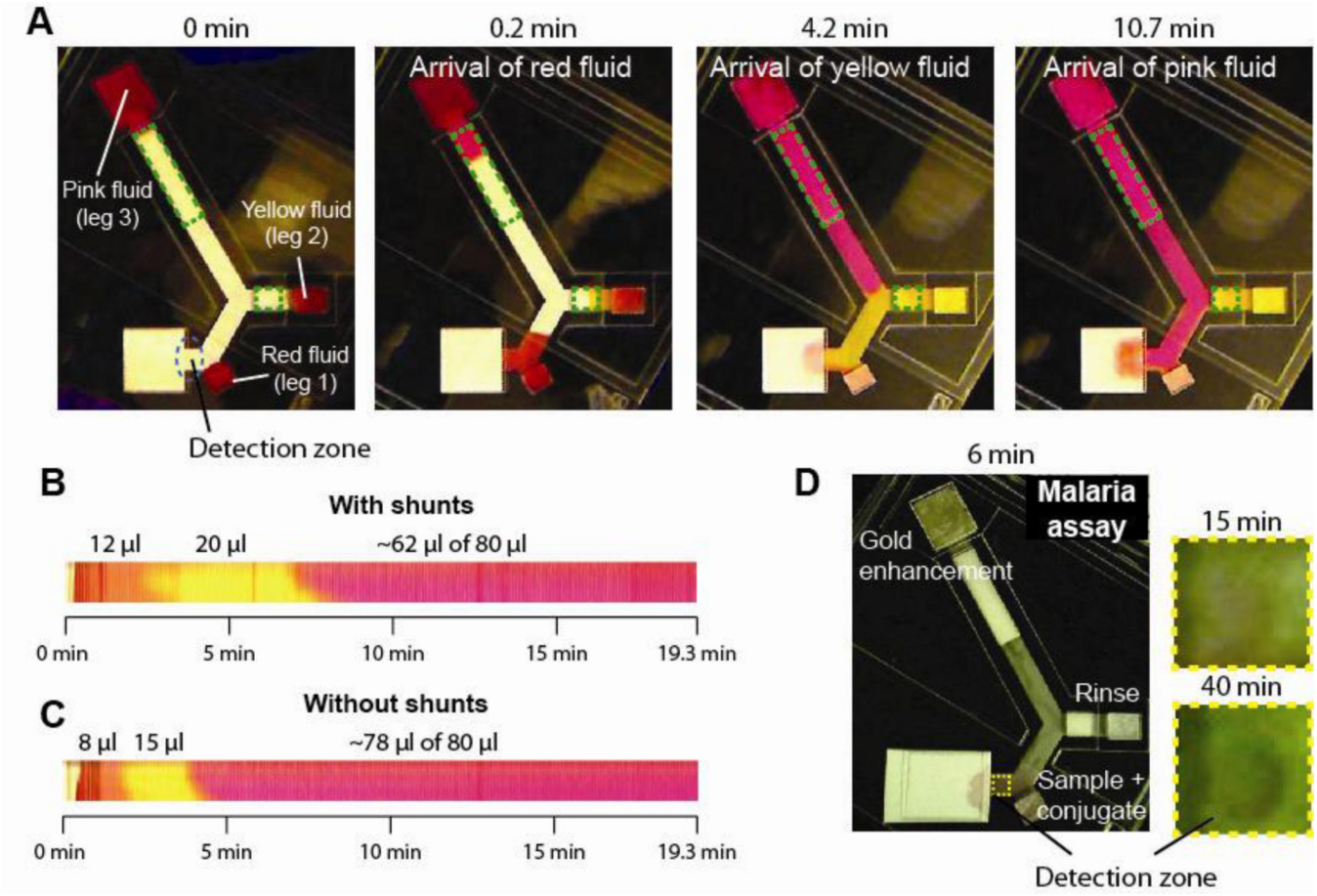

Figure 5.

Sequential delivery of fluids using shunts. **A**. Time-lapse images of a folding-card device for the sequential delivery of red, yellow, and pink fluids to a detection zone. Legs 2 and 3 of the device contained cellulose CFSP223000 shunts, outlined by the dotted green lines, of length 5.1 mm and 20.3 mm, respectively. All legs were 4.6 mm wide. **B-C**. Montages of a portion of the detection zone, a sub-region within the dotted blue lines, of a device containing shunts (**B**) and not containing shunts (**C**). The shunts enabled delivery of larger volumes of fluid to the detection zone. **D**. Folding-card device for the feasibility demonstration of amplified detection of the malaria protein *Pf*HRP2. Antigen plus gold-antibody conjugate, a rinse solution, and a gold enhancement solution were sequentially delivered to the detection zone. The original pink signal obtained at 15 minutes was amplified to a blue-black signal by 40 minutes.